Chemistry–A European Journal
Research Article
doi.org/10.1002/chem.202301005
Chemistry Europe
European Chemical Societies Publishing
www.chemeurj.org

Challenges in the Direct Detection of Chirality-induced Spin Selectivity: Investigation of Foldamer-based Donor-acceptor Dyads

Alberto Privitera,*[a, c] Davide Faccio,[d] Demetra Giuri,[d] Elisabeth I. Latawiec,[e] Damiano Genovese,[d] Francesco Tassinari,[f] Liviana Mummolo,[d] Mario Chiesa,[c] Claudio Fontanesi,[g] Enrico Salvadori,[c] Andrea Cornia,[f] Michael R. Wasielewski,[e] Claudia Tomasini,*[d] and Roberta Sessoli*[b]

Dedicated to Prof. Maurizio Prato on the occasion of his 70th birthday.

Over the past two decades, the chirality-induced spin selectivity (CISS) effect was reported in several experiments disclosing a unique connection between chirality and electron spin. Recent theoretical works highlighted time-resolved Electron Paramagnetic Resonance (trEPR) as a powerful tool to directly detect the spin polarization resulting from CISS. Here, we report a first attempt to detect CISS at the molecular level by linking the pyrene electron donor to the fullerene acceptor with chiral peptide bridges of different length and electric dipole moment. The dyads are investigated by an array of techniques, including cyclic voltammetry, steady-state and transient optical spectroscopies, and trEPR. Despite the promising energy alignment of the electronic levels, our multi-technique analysis reveals no evidence of electron transfer (ET), highlighting the challenges of spectroscopic detection of CISS. However, the analysis allows the formulation of guidelines for the design of chiral organic model systems suitable to directly probe CISS-polarized ET.

Introduction

Chirality plays an essential role in several disciplines ranging from life science and chemistry to physics and material science.[1] Most recently, the concept of chirality has received significant attention following the observation of the so-called chirality-induced spin selectivity (CISS) effect.[2] The CISS effect has disclosed a fundamental link between chirality and the electron's spin angular momentum.[3] In a nutshell, when the electron passes through a chiral molecule or material, transmission is favored for a certain spin polarisation, which depends on the handedness of the medium.[4] This phenomenon is of paramount interest since it can induce high spin polarisation even at room temperature[5] and can set the stage for novel applications in spintronics and quantum information technologies.[6]

In the last few decades, the CISS effect has been observed in several phenomena, such as the response of magnet-free

[a] Dr. A. Privitera
Department of Industrial Engineering
University of Florence
Via Santa Marta 3, 50139 Firenze (Italy)
E-mail: alberto.privitera@unifi.it

[b] Prof. R. Sessoli
Department of Chemistry "U. Schiff" and INSTM Research Unit
University of Florence
Via della Lastruccia 3–13, 50019 Sesto Fiorentino (Italy)
E-mail: roberta.sessoli@unifi.it

[c] Dr. A. Privitera, Prof. M. Chiesa, Prof. E. Salvadori
Department of Chemistry and NIS Centre
University of Torino
Via Pietro Giuria 7, 10125 Torino (Italy)

[d] Dr. D. Faccio, Dr. D. Giuri, Dr. D. Genovese, Dr. L. Mummolo, Prof. C. Tomasini
Department of Chemistry "Giacomo Ciamician"
University of Bologna
Via Selmi 2, 40126 Bologna (Italy)
E-mail: claudia.tomasini@unibo.it

[e] E. I. Latawiec, Prof. M. R. Wasielewski
Department of Chemistry, Center for Molecular Quantum Transduction and Paula M. Trienens Institute for Sustainability and Energy
Northwestern University
Evanston, IL 60208-3113 (USA)

[f] Dr. F. Tassinari, Prof. A. Cornia
Department of Chemical and Geological Sciences and INSTM Research Unit
University of Modena and Reggio Emilia
Via G. Campi 103, 41125 Modena (Italy)

[g] Prof. C. Fontanesi
Department of Engineering "E. Ferrari"
University of Modena and Reggio Emilia
Via P. Vivarelli 10, 41125 Modena (Italy)

Supporting information for this article is available on the WWW under https://doi.org/10.1002/chem.202301005

spintronic devices,[6b,7] spin-dependent photoluminescence,[8] enantiomeric enrichment,[9] enantiospecific electrochemistry,[10] and spin selectivity in photoelectrochemical water splitting.[11] However, almost all these experiments relied on the fabrication of hybrid interfaces between chiral molecules and inorganic substrates acting as electrodes, thereby providing solely an indirect observation of CISS. Only recently, a few research groups have focused their attention on the direct detection of the CISS effect at the molecular level.[6a,7,12] In principle, this could be achieved by probing the spin polarisation arising from photoinduced electron transfer (ET) in D-χ-A architectures, where D is an electron donor, A is an electron acceptor, and χ is a chiral bridge.[6a,7,12a,c,13] For these studies, time-resolved Electron Paramagnetic Resonance (trEPR) is the technique of choice, as it allows to probe any CISS-dependent signature on the behaviour of the photogenerated radical pairs, including their coherent spin dynamics.[6a,12b,c,14] Interestingly, trEPR measurements also have great potential for studying CISS in randomly oriented samples.[12a] If successful, the direct detection of the CISS effect via EPR spectroscopy will promote the development of a more robust theoretical description of the phenomenon, with no need to model interfaces, and the formulation of clear and handy guidelines for the synthesis of CISS-active materials. Behind the excitement of these promises, however, lays the stark reality. In fact, the quasi-totality of the available results comes from theoretical works,[6a,13b,14,15] and the very few experimental attempts present in the literature are not conclusive yet.[12a] The main challenge originates from the complexity of developing model systems exhibiting at the same time good ET efficiency, effective chiral spin filtering, and charge transfer (CT) states lasting hundreds of ns, as required for trEPR investigation.[12a]

Our previous work identified a hybrid organic-inorganic system comprising a CdSe quantum dot (QD) and C_{60} fullerene (C_{60}) as D and A, respectively, covalently linked through a saturated oligopeptide helical bridge (χ).[12a] Although this architecture looks promising, the photoexcited state of the inorganic QD has complex spin properties. As a result, it is difficult to discriminate whether the observed spin-polarisation arises from a CISS-mediated ET or a standard ET. In parallel to the QD approach, which as of now remains the most investigated one,[7] it is crucial to develop new chiral systems where an organic D replaces the inorganic QD. This approach enables not only to simplify the excited state physics of the D, but also to finely tune its properties by chemical modification. In addition, purely organic D-A systems are often characterized by negligible spin-orbit coupling (SOC), whose impact on the spin selectivity of ET can thus be disclosed by comparison.[7,12b]

Here, we prepare and investigate novel D-χ-A systems (from now on called dyads) that combine two key concepts needed for the direct observation of CISS: (1) fully organic D and A moieties with well-defined photophysical properties, namely pyrene (D) and C_{60} (A); (2) chiral saturated peptide bridges (χ) of different length and electric dipole moment, known to act as efficient spin filters in spintronic devices.[4b,8,16] With these dyads in hand, we investigate the effect of the chiral bridge on the reduction and oxidation potentials of the D and A moieties via cyclic voltammetry (CV). In addition, through a detailed spectroscopic investigation, including time-resolved photoluminescence (trPL), trEPR, and transient absorption (TA) experiments, we highlight the strengths and weaknesses of our novel fully-organic dyads. Finally, we propose guidelines for the design of chiral organic model systems suitable for the direct observation of the CISS effect.

Results and Discussion

Dyads building blocks

To optimize the photoinduced ET process, which is key for efficient detection of the CISS effect via trEPR,[12a] we engineered our D-χ-A dyads with the pyrene (Py) and C_{60} units acting as D and A, respectively. Py is a very attractive chromophore due to its intrinsic optical properties, such as high photoluminescence (PL) quantum yield, long fluorescence lifetimes, and controlled formation of excimers and aggregates, which made it one of the most studied fluorescent probes in macromolecules and nanostructured systems.[17] In addition, it is an excellent D and has been used as an antenna chromophore in dyads with C_{60} for solar energy conversion applications.[18] Its long singlet lifetime ensures that when Py is coupled with an A, the photoinduced ET occurs from a singlet excited state, significantly simplifying the interpretation of the spin polarisation arising from the ET.[18d] C_{60} has excellent A abilities thanks to its low-lying unoccupied molecular orbitals and the small reorganization energy in the ET process.[19] As a result, C_{60} derivatives have played a fundamental role in the design of photoactive D-A dyads and triads, and in the organic photovoltaic field.[12b,18a,20] Furthermore, the very small spectral overlap between Py emission and C_{60} absorption rules out the possibility of an efficient Fluorescence Resonance Energy Transfer (FRET) from Py to C_{60}, in favor of the ET process.[18a]

Turning to the chiral bridges, peptide chains are known to promote high spin selectivity in CISS-based spintronic devices.[3,4,8,16,21] The chiral bridges used herein are based on the L-Ala-D-Oxd repeating unit, where L-Ala is L-alanine and D-Oxd is the pseudo amino acid (4*R*,5*S*)-4-carboxy-5-methyloxazolidin-2-one. These peptides can form well-organized 3_{10} helices when the number of repeating units is higher than five, as demonstrated by the enhancement of the circular dichroism.[22] In addition, earlier DFT calculations have indicated that the geometry of these bridges is preserved after bonding to the fulleropyrrolidine.[12a] This was computed for bridge lengths of 4 amino acids and most likely holds true for longer bridges as well, where several hydrogen bonds further stabilize the secondary structure. The bridge stiffness is important for reducing the system's conformational freedom, which is needed when developing benchmark CISS systems.[23]

Different spacer lengths, i.e., 4, 10, and 14 amino acids, were probed to investigate the trade-off between ET and spin filtering efficiency. In addition, since literature results show that the direction of the electric dipole of the bridge can have a profound impact on ET efficiency,[24] two different types of

dyads – hereafter referred to as "direct" and "inverse" – were investigated. In "direct" dyads (Dir), the electric dipole of the peptide chain is parallel to the ET direction (from Py to C_{60}), while in inverse dyads (Inv) it is antiparallel. Six different dyads were thus synthesized, namely **Dir4**, **Dir10**, **Dir14**, **Inv4**, **Inv10**, and **Inv14**, where the digit indicates the number of amino acids (Figure 1).

Synthesis of the dyads

All the molecules were prepared by liquid phase synthesis, starting from commercially available L-alanine, D-threonine, C_{60}, and Py derivatives. The functionalization of C_{60} was successfully obtained according to the Prato reaction,[25] with either a carboxyl group derivative for direct dyads or an amino group for inverse dyads (Schemes S1–S4 in Supporting Information). The bridges were prepared by peptide coupling with good to excellent yields.

For the preparation of direct dyads **Dir4**, **Dir10**, and **Dir14**, (*N*-methyl)-fulleroproline *t*-butyl ester was synthesized according to the conditions reported in the literature for similar compounds[25] and coupled with one L-Ala-D-Oxd-OBn unit, forming (*N*-methyl)-fulleroproline-L-Ala-D-Oxd-OBn. The bridges of different length were derivatized, replacing the OBn protecting group with 1-(bromomethyl)pyrene. Finally, the two chains holding the fulleroproline unit at the *N*-terminal position and the Py unit at the *C*-terminal position were deprotected and coupled, giving the required dyads, with good yield after careful purification. For further details, chemical yields, and characterizations, see Supporting Information (Scheme S1).

To prepare the inverse dyads **Inv4**, **Inv10**, and **Inv14**, C_{60} was derivatized to Boc-*N*-aminoethyl-*N*-fulleropyrrolidine, following a known procedure,[25] then the *N*-Boc protecting group was removed and replaced with one L-Ala-D-Oxd-OBn unit, to furnish Boc-L-Ala-D-Oxd-*N*-2-aminoethyl-fulleropyrrolidine (Scheme S2). The inverse dyads **Inv4** and **Inv10** were prepared by coupling this derivative with two bridges holding a carboxypyrene group, namely pyrenecarbonyl-L-Ala-D-Oxd-OBn for **Inv4** and pyrenecarbonyl-(L-Ala-D-Oxd)$_4$-OBn for **Inv10**. After removal of the protecting groups, peptide coupling, and purification, the two dyads were obtained in good overall yields (Scheme S3). The dyad **Inv14** was prepared in a similar way, coupling Boc-L-Ala-D-Oxd-*N*-2-aminoethyl-fulleropyrrolidine with 4-pyren-1-yl-butanoyl-L-Ala-D-Oxd-OBn. After removal of the protecting groups, peptide coupling, and purification, this third inverse dyad was obtained in good overall yield (Scheme S4). For our purposes, the use of a 4-(pyren-1-yl)-butanoate group, replacing the pyrene-1-carboxylate group (used for **Inv4** and **Inv10**) affects the photophysical properties only marginally, as shown below.

Three short-chain control compounds carrying a Py termination but no C_{60} group were also synthesized and employed

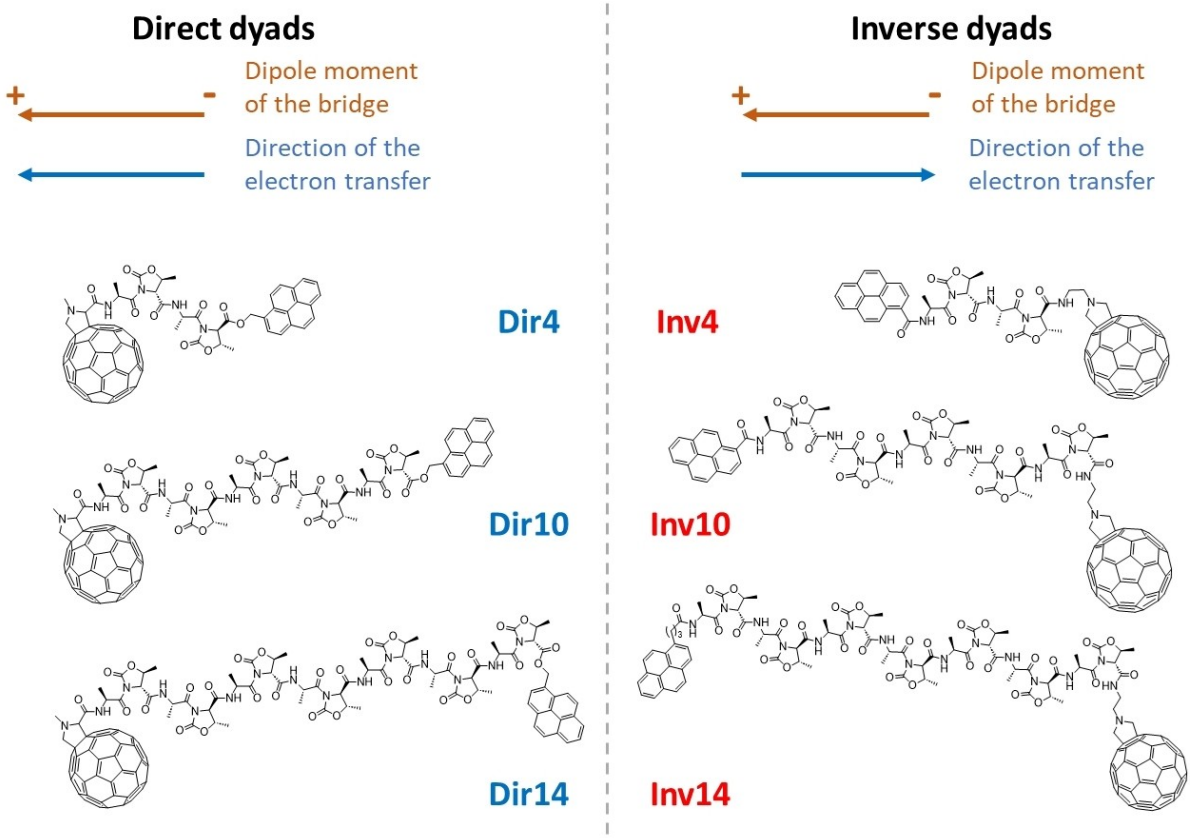

Figure 1. Engineering of the D-χ-A dyads. Sketched molecular structures of the six D-χ-A dyads synthesised in this work. The Py unit acts as an electron donor (D) and the C_{60} unit as an electron acceptor (A). Different chiral bridges have been probed to investigate the role of the bridge length and its electric dipole moment. Legend: Dir = direct dyad, i.e., the electric dipole moment of the bridge is parallel to the direction of ET; Inv = inverse dyad, i.e., the electric dipole moment of the bridge is antiparallel to the direction of ET; n = number of amino acids of the peptide bridge.

as control systems for the electrochemical and photophysical measurements, namely **Py-Dir** (Scheme S1), **Py-Inv** (Scheme S3), and **Py-Inv′** (Scheme S4). **Py-Dir** is the control compound for the three direct dyads (**Dir4**, **Dir10**, and **Dir14**), **Py-Inv** is the control compound for the short (**Inv4**) and intermediate (**Inv10**) inverse dyads, and **Py-Inv′** is the control compound for the long inverse dyad (**Inv14**). Their synthesis and characterization are reported in Supporting Information.

Electrochemical measurements

CV measurements in DMSO/toluene (1:1 v/v) were performed on **Dir4**, **Inv4**, **Dir10**, and **Inv10** dyads, as well as on the short-chain control compounds **Py-Dir** and **Py-Inv**. Figure 2 sets out a representative CV, recorded on **Inv4** dyad; the whole set of experimental CVs can be found in the Supporting Information (Figures S1–S8).

The electrochemical response of the C_{60} group is clearly observable in all four dyads, which exhibit three well-differentiated reversible reduction peaks at $E^{(1/2)}_{red1}$ ~−0.6 V, $E^{(1/2)}_{red2}$ ~−1.0 V, and $E^{(1/2)}_{red3}$~−1.6 V (vs. Fc^+/Fc, see Table 1). Differences between compounds are minimal: all three reduction potentials of **Dir4** are slightly more negative than those of the remaining dyads, while **Dir10** and **Inv10** have the least negative value of $E^{(1/2)}_{red1}$. All investigated compounds, including **Py-Dir** and **Py-Inv**, exhibit a reversible peak at $E^{(1/2)}_{red4}$~−2.2 V that we attribute to the reduction of the Py group.[26] Here, reduction potentials are essentially the same in the four dyads and in **Py-Inv**, while **Py-Dir** is slightly easier to reduce. The redox properties of the terminal redox groups may be modulated both by substituent effects and by the orientation of the electric dipole moment,[24a] which is opposite in direct vs. inverse dyads (Figure 1). Due to the attachment of the carbonyl carbon to the fulleropyrrolidine moiety, the C_{60} group should be easier to reduce in direct than in inverse dyads. For the same reason, reduction of Py group should be significantly easier in inverse than in direct structures.[26] Electric dipole moment orientation would further contribute to making direct structures easier (harder) to reduce at C_{60} (Py) termination as compared with their inverse counterparts. Clearly, the reduction potentials in Table 1 do not follow these predictions, suggesting that the redox properties of our dyads and control compounds are not primarily ruled by substituent and dipole moment effects.

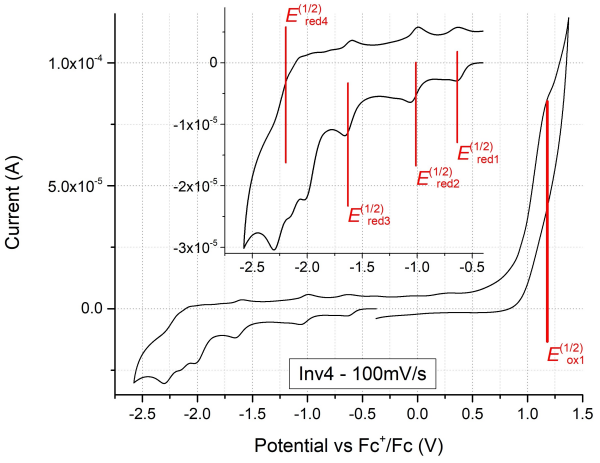

Figure 2. Representative CV of **Inv4** (1 mM) recorded in DMSO/toluene (1:1 v/v) at a scan rate of 100 mV/s with 0.1 M tetra-*n*-butylammonium tetrafluoroborate ($TBABF_4$) electrolyte. Fc^+/Fc is the ferrocenium/ferrocene redox couple.

The anodic portion of the CV is less resolved, and the recorded current values indicate multiple overlapping irreversible oxidation processes that occur in the 1.0–1.3 V vs. Fc^+/Fc potential range. In this potential window, one expects oxidation of both Py and amide moieties.[26] In particular, in their classical work O'Donnell and Mann report oxidation potentials of 0.8–1.1 and 1.4 V vs. Fc^+/Fc for tertiary and secondary aliphatic amides, respectively.[27] The best-defined anodic peak before the onset of solvent oxidation gives $E^{(1/2)}_{ox1}$~1.2 V (Table 1). Combining this value with the $E^{(1/2)}_{red1}$ reduction potential of C_{60} (~−0.6 V) yields an electrochemical difference of ca. 1.8 V for the four dyads investigated, which can be transformed into a 1.8 eV HOMO–LUMO gap. The electrochemical HOMO–LUMO gap for Py group, estimated as $E^{(1/2)}_{ox1}$–$E^{(1/2)}_{red4}$, is ca. 3.4 V, in agreement with literature data,[26] and matches well the reported optical bandgap (ca. 3.45 V).[28] This analysis evidences that the C_{60} LUMO is lower in energy than the Py LUMO and therefore suggests that the ET process is, in principle, favored for all the dyads without significant differences between direct and inverse ones or linkers with different length.

Table 1. Half-wave potential values and electrochemical HOMO–LUMO gaps (V) for 1 mM solutions of dyads and control compounds in DMSO/toluene (1:1 v/v) with 0.1 M $TBABF_4$.[a]

Compound	$E^{(1/2)}_{red1}$	$E^{(1/2)}_{red2}$	$E^{(1/2)}_{red3}$	$E^{(1/2)}_{red4}$	$E^{(1/2)}_{ox1}$[b]	$E^{(1/2)}_{ox1}-E^{(1/2)}_{red1}$[c]	$E^{(1/2)}_{ox1}-E^{(1/2)}_{red4}$[d]
Dir4	−0.66	−1.09	−1.70	−2.18	1.22	1.88	3.40
Inv4	−0.62	−1.02	−1.62	−2.19	1.17	1.79	3.36
Dir10	−0.58	−1.03	−1.64	−2.18	1.27	1.85	3.45
Inv10	−0.58	−1.02	−1.61	−2.19	1.13	1.71	3.32
Py-Dir	–	–	–	−2.14	1.23	–	3.37
Py-Inv	–	–	–	−2.18	1.14	–	3.32

[a] vs. the Fc^+/Fc redox couple. [b] Estimated from the inflection points of the anodic waves for the irreversible oxidation peaks. [c] Electrochemical HOMO–LUMO gap for the dyad. [d] Electrochemical HOMO–LUMO gap for Py group.

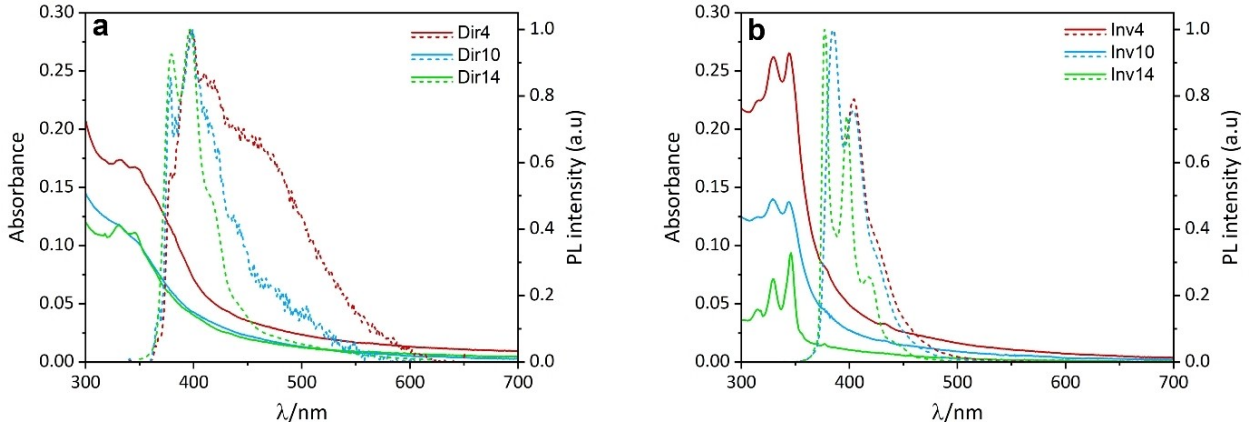

Figure 3. Absorption and emission spectra of D-χ-A dyads in DMSO at room temperature. Absorption (solid lines) and emission spectra (dashed lines) of a) direct and b) inverse dyads. Emission spectra were measured with $\lambda_{exc}=330$ nm and normalized at their maximum.

UV-vis absorption and PL measurements

We investigated the photophysical properties of our samples in solution by combining UV-vis absorption and PL spectroscopy (Figures 3 and S9). We carried out the measurements in pure DMSO (approximate concentration 5 μM), a better solvent for the dyads compared to chlorinated solvents, DMF, toluene, and other non-polar media. UV-vis spectra of both the direct and inverse dyads show the characteristic absorption bands of Py and C_{60}. The spectra in Figure 3 suggest that the D/A units have independent optical absorptions,[18a] likely due to the hindered electronic communication between the two terminal chromophores through a peptide bridge. The result is further corroborated by PL spectra, which show the dominant emission of the Py unit, as expected considering the relative PL efficiency between Py and C_{60}. In addition to Py emission, the PL spectra of **Dir4** and **Dir10** (Figure 3a) feature a significant broad band centered at longer wavelengths (~470 nm) and ascribable to the presence of aggregates arising from the poor solubility of these dyads.[29] Conversely, **Dir14** and all the inverse dyads show purely monomeric emission spectra without traces of excimers or aggregates (Figure 3b).

To gain further insight into the photophysics of the dyads in solution and probe any photoinduced ET between the Py and C_{60} units, we measured PL quantum yields (Φ_{PL}) and performed trPL experiments on all dyads and the three control compounds. The data in Table 2 reveal that PL quenching is stronger in the three direct dyads ($\Phi_{PL}=0.016$, 0.004, and 0.030 in **Dir4**, **Dir10**, and **Dir14**, respectively) than in the corresponding control compound **Py-Dir** ($\Phi_{PL}=0.25$). The PL quantum yield is reduced less dramatically in the inverse dyads **Inv4** and **Inv10** ($\Phi_{PL}=0.20$ and 0.30, respectively) compared to **Py-Inv** ($\Phi_{PL}=0.58$), and in **Inv14** ($\Phi_{PL}=0.24$) vs. **Py-Inv′** ($\Phi_{PL}=0.33$).

Table 2. PL quantum yields (Φ_{PL}) and PL lifetimes (τ_n) and amplitudes (B_n) of dyads and control compounds, with $\lambda_{exc}=330$ nm for both PL quantum yield measurements and trPL experiments; the decay time at $\lambda_{em}=465$ nm (τ_{465}) was measured for the dyads **Dir4** and **Dir10** featuring excimer emission band, with rise times τ_{RISE} indicated by the negative amplitude B_{465}.

Sample	Φ_{PL}	τ_{395} [ns] (B_{395})	τ_{465} [ns] (B_{465})
Py-Dir	0.25	$\tau_1=84.9$	
Dir4	0.016	$\tau_3=0.51$ (515) $\tau_2=8.2$ (486) $\tau_1=47.5$ (63)	$\tau_{RISE}=0.15$ (−370) $\tau_{Agg,2}=4.6$ (496) $\tau_{Agg,1}=17.4$ (508)
Dir10	0.004	$\tau_3=0.40$ (635) $\tau_2=7.7$ (525) $\tau_1=51.8$ (112)	$\tau_{RISE}=0.31$ (−1286) $\tau_{Agg,2}=4.3$ (817) $\tau_{Agg,1}=15.1$ (350)
Dir14	0.030	$\tau_2=8.5$ (607) $\tau_1=80.0$ (329)	
Py-Inv	0.58	$\tau_1=22.5$	
Inv4	0.20	$\tau_2=3.6$ (57) $\tau_1=22.0$ (892)	
Inv10	0.30	$\tau_1=22.4$	
Py-Inv′	0.33	$\tau_1=79.2$	
Inv14	0.24	$\tau_2=11.2$ (112) $\tau_1=79.1$ (852)	

The PL decay curves of the direct dyads obtained at λ_{em} = 395 nm (i.e., monitoring the monomer emission) show multi-exponential kinetics. Quenching of excited states due to electronic interactions in aggregates, including excimer formation, is commonly very fast and occurs in the sub-ns time range.[30] This type of fast quenching is observed in dyads **Dir4** and **Dir10**, which also show the excimer emission band typical of aggregation (Figure 3a). In addition, the presence of rise times (τ_{RISE}) that span the same sub-ns time scale in the trPL of excimer emission monitored at 465 nm further confirms the critical presence of aggregation for these two dyads. This analysis allows confining the effect of quenching due to aggregation to the sub-ns time region and discussing the longest components of trPL in the perspective of quenching due to other possible mechanisms, for example energy transfer or ET. Specifically, the longest time is τ_1 = 47.5, 51.8, and 80.0 ns for **Dir4**, **Dir10**, and **Dir14**, respectively, to be compared to 84.9 ns for control compound **Py-Dir** where C_{60} is absent. This may reflect a partial quenching due to either energy transfer or ET occurring through the chiral bridge. According to the amplitudes of these components of the decay, the mentioned ET efficiencies concern only a fraction of dyads amounting to 6%, 9%, and 35% for dyads **Dir4**, **Dir10**, and **Dir14**, respectively. The intermediate time (τ_2 = 8.2, 7.7, and 8.5 ns for **Dir4**, **Dir10**, and **Dir14**, respectively) can be tentatively assigned to a side quenching process independent from the bridge length, like that expected to occur in folded conformers where D and A are brought in closer contact.

From the trPL analysis of the inverse dyads, we obtain no clear evidence of aggregation, confirming the absence of excimer emission from these samples (Figure 3b). The most significant component of the decay has the same lifetime as the corresponding control compound (τ_1 = 22.0, 22.4, and 79.1 ns in **Inv4**, **Inv10**, and **Inv14** to be compared to 22.5 ns in **Py-Inv** and 79.2 ns in **Py-Inv′**), suggesting that no quenching process takes place. However, **Inv4** and **Inv14** show minor quenching contributions with τ_2 = 3.6 ns and 11.2 ns, respectively, that we attribute to at least one molecular conformation exhibiting a moderate quenching.

TrEPR measurements

We carried out trEPR spectroscopy to elucidate the origin of trPL quenching and evaluate the presence of a spin-polarised photoinduced ET. We performed the measurements on **Dir14** and on the three inverse dyads (**Inv4**, **Inv10**, and **Inv14**) since these four compounds do not show any evidence of aggregation via optical analysis. Aggregation would result in intermolecular ET and therefore impair our analysis. All the dyads were dissolved in DMSO/toluene (1 : 1 v/v) at 20 μM concentration and photoexcited with a 355 nm laser pulse. All the spectra were acquired at T = 50 K because measurements in fluid solution would undermine the detection of CISS due to motional averaging.[6a] In Figure 4, we show the trEPR spectra of the four dyads (black lines) acquired at 1 μs after the laser pulse, along with the spectrum of the CdSe QD-χ-C_{60} system (blue line) studied in our recent publication,[12a] as a comparison for the ET. Notably, the signals of both the C_{60} radical anion and the counterpart radical cation would be expected in organic dyads.[12b] The full 2D experimental trEPR contour plots of the four dyads are available in Figure S12. In all the studied dyads, we observe a broad signal between 335 and 358 mT. Based on the spectral simulation (red line) in Figure 4, we assign this signal to the standard C_{60} triplet state (^{3}*C_{60}) formed via intersystem crossing (ISC) promoted by SOC.[31] However, while the CdSe QD-χ-C_{60} system exhibits an additional signal due to the photoinduced C_{60} anion,[12a] none of the organic dyads do. This observation indicates that a photoinduced ET able to generate a spin-polarised long-lived CT state is not occurring in our fully organic dyads at 50 K.

TA measurements

Both our CV measurements and previous literature results suggest that Py/C_{60} should be, in principle, a good D/A couple due to the favourable HOMO–LUMO alignment.[17,18] In addition, our trPL experiments suggest some degree of PL quenching at room temperature for most of the studied dyads. The absence of a trEPR signal due to photoinduced ET can be caused by a variety of factors other than a lack of ET, such as fast charge recombination. With the aim of rationalizing our observation and providing a complete photophysical picture of our dyads, we performed TA experiments on the two shortest dyads (**Dir4** and **Inv4**) and the respective control compounds (**Py-Dir** and **Py-Inv**).

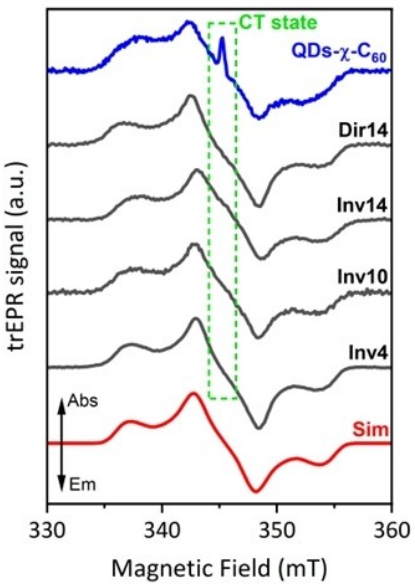

Figure 4. trEPR spectra of D-χ-A dyads. Normalized experimental trEPR spectra of **Dir14**, **Inv4**, **Inv10**, and **Inv14** (black lines) taken at 1 μs after a 355 nm laser pulse (7 ns, 2 mJ). The spectra are acquired at 50 K. All spectra show a broad signal in the magnetic field range 335–358 mT, which is assigned to the C_{60} triplet based on the best-fit spectral simulations (red line). The simulation parameters are reported in Table S1. As a comparison for the ET, the trEPR spectrum of the CdSe QD-χ-C_{60} system (blue line) is also plotted.[12a] Arrows legend: Abs = enhanced absorption, Em = emission.

Selective photoexcitation of Py at 350 nm in the control molecules resulted in similar femtosecond transient absorption (fsTA) spectra (Figures S14a and S15a). Each molecule shows strong excited state absorption (ESA) bands at 390 and 500 nm that are typical of ^{1}*Py.[32] Given that these systems are conformationally flexible, some excited state relaxation occurs in 66 and 157 ps for ^{1}***Py-Dir** and ^{1}***Py-Inv**, respectively (Figures S14b and S15b). The ESA features in each case live beyond the 8-ns pump-probe delay limit of the fsTA apparatus. The nanosecond transient absorption (nsTA) spectra of **Py-Dir** and **Py-Inv** also show similar features resulting from the decay of ^{1}***Py-Dir** and ^{1}***Py-Inv** to form ^{3}***Py-Dir** and ^{3}***Py-Inv**, respectively (Figures S13a and S13c). Global fits to the data show that ^{1}*Py decays with a 25 ns lifetime in both molecules (Figure S13b and d). However, the ESA spectra of **Py-Dir** exhibit a 164-ps decay component with spectral characteristics of both ^{1}*Py and ^{3}*Py (Figure S13b). This component may be due to conformational flexibility at the methylene group linking Py to the peptide. This feature is notably absent in the ESA spectra of **Py-Inv** (Figure S13d), which has a stiffer carboxamide linker to the peptide. Both ^{3}***Py-Dir** and ^{3}***Py-Inv** decay in about 100 μs. Further nanosecond kinetics at selected wavelengths and time-dependent populations for **Py-Dir** and **Py-Inv** are shown in Figure S16.

The fsTA spectra of **Dir4** show the initial formation of ^{1}*Py (Figure S17a), except that the spectra are complicated by co-excitation of C_{60} at 350 nm, which results in a ground state bleach of the C_{60} ground state absorption at 375 nm. The fsTA spectrum also shows a band at 900–1000 nm that results from the formation of ^{1}*C_{60}.[33] The A and B components in the fsTA ESA spectra show that ^{1}*C_{60} decays to ^{3}*C_{60} in about 1.5 ns with the dominant ^{3}*Py absorption features persisting on a time scale ⩾ 8 ns (Figure S17b). The fsTA spectra of **Inv4** show similar spectral features (Figure S18a), which decay with complex kinetics resulting from co-excitation of Py and C_{60}. Once again, both ^{3}*Py and ^{3}*C_{60} are evident on the 8-ns timescale (Figures S18a and S18b).

The nsTA spectra of **Dir4** and **Inv4** show clear differences at long times (Figure 5a and c). The spectra of **Dir4** at times less than ~1 μs show that both ^{3}*Py and ^{3}*C_{60} are present, while at later times only ^{3}*C_{60} remains as evidenced by the bleach at 375 nm. This is consistent with energy transfer from ^{3}*Py to C_{60} to produce ^{3}*C_{60}, given that the energies of ^{3}*Py and ^{3}*C_{60} are 2.1 eV[34] and 1.6 eV,[35] respectively. In contrast, the nsTA spectra of **Inv4** clearly show that ^{3}*Py initially dominates over ^{3}*C_{60} as the spectra strongly resemble those of **Py-Inv**. Due to its clear EPR fingerprint, ^{3}*C_{60} is still detectable via trEPR.[20e,31] In this case, as in **Py-Inv**, ^{1}*Py decays in 23 ns to form ^{3}*Py followed by decay of the triplet to ground state in 15 μs. Further nanosecond kinetics at selected wavelengths and time dependent populations for **Dir4** and **Inv4** are shown in Figure S19. The greater excitation selectivity of Py over C_{60} in the case of **Inv4**

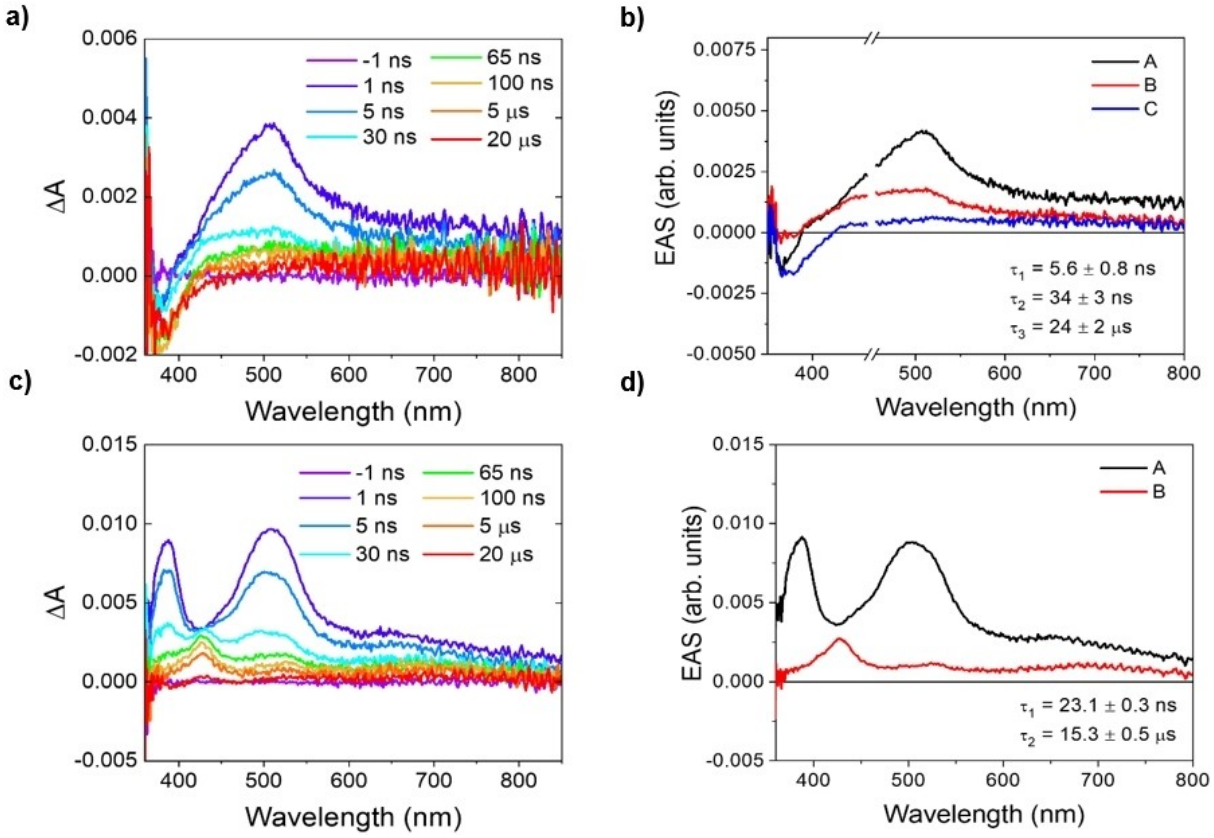

Figure 5. Room temperature nsTA spectra in DMSO/toluene (1 : 1 v/v) excited at 350 nm recorded at selected delay times. a, c) spectra of **Dir4** and **Inv4**, respectively. b, d) Evolution-associated spectra (EAS) of **Dir4** and **Inv4**, respectively, assuming an A→B→C mechanism A→B occurs with τ_1 and B→C occurs with τ_2.

most likely results from a shift in the absorption maximum of the Py-carboxamide relative to that of the methylene-substituted Py.

In summary, the fsTA and nsTA spectra and kinetics of **Dir4** and **Inv4** corroborate the trEPR observations and show no evidence for significant ET from ^{1}*Py to C_{60} to produce $Py^{\bullet+}$-$C_{60}^{\bullet-}$.

Discussion

Although peptide helices are known to mediate long-range ET between D/A moieties,[36] to our knowledge multi-technique investigations of this process are unprecedented. Indeed, most literature studies of ET in helical structures were based on optical or electrochemical techniques and mainly aimed at understanding how redox processes occur in biochemical reactions and at controlling them in related synthetic systems.[36,37] As of now, the nature of long-range ET in D-A dyads connected by a peptide bridge is still debated, and two different mechanisms have been proposed: (1) a superexchange mechanism, consisting in a coherent electron tunneling in which the peptide bridge tunes the tunneling barrier height and thus the electronic coupling between D and A; (2) a sequential hopping mechanism, consisting in an incoherent, multi-tunneling process that involves the bridge orbitals directly. All studies highlighted the complex nature of the ET process due to several critical parameters, such as the nature of the peptide structure, the hydrogen bonds, the surrounding medium, and conformational fluctuations.[38]

Turning to the trEPR experiments, most studies on radical pairs generated via photoinduced ET relied on ultrafast multi-step ET processes that ensure good ET efficiency and a long lifetime of the photogenerated CT state.[12b] Examples can be found in nature, for example in photosynthetic reaction center proteins,[39] and in D-A-A′ triads, where the first charge separation is photodriven, while the second is thermally allowed.[40] Alternatively, good ET efficiencies and slow recombination rates have been achieved in D-A dyads by finely tuning unsaturated bridges to promote good electronic communication between D and A, while keeping them sufficiently apart to slow down charge recombination.[41] In our case, trEPR measurements, supported by TA experiments, do not reveal any sign of ET, most likely as a consequence of the long sequence of single bonds linking ^{1}*Py to C_{60}, which is known to strongly attenuate through-bond ET processes.[42]

Interestingly, previous research has shown that similar chiral bridges exhibit good CISS filtering properties not only in spintronic devices, where electron transport occurs via an external electric field,[23] but also in photodriven D-A dyads composed of two CdSe QDs templated on silica microbeads.[21] In the latter case, a spin-polarized photoinduced ET has been observed via time-correlated single photon counting technique using circularly-polarized excitation light. Furthermore, our prior trEPR studies on CdSe QDs-χ-C_{60} systems revealed the presence of a spin-polarized photoinduced ET consistent with the CISS effect.[12a] This implies that peptide linkers have the potential for photoinduced CISS studies in hybrid organic-inorganic D-A systems. Nevertheless, our current results suggest that fully organic dyads operate rather differently. According to our electrochemical investigation, the frontier energy levels of our dyads show that the standard free energy change (ΔG^0) for photoinduced ET is strongly negative, yet no ET is observed.

In classical terms, the ET rate can be described by the Marcus equation,[37c] which is characterized by various key parameters: (i) ΔG^0 for ET; (ii) the reorganization energy (λ) required for structural and environment relaxation upon ET, and (iii) the electronic coupling matrix element between D and A (V_{DA}), which typically decreases exponentially with the distance (R_{DA}) between D and A, i.e. $V_{DA} = V_0 \exp(-\beta R_{DA})$ where V_0 is the electronic coupling at $R_{DA} = 0$. The attenuation factor β appearing in the above equation is more than just a bridge-specific constant and is affected by D and A.[43] This most likely explains why, despite having the same chiral bridge and acceptor and a favorable ΔG^0 for ET, pyrene- and QD-based chiral dyads behave differently. Furthermore, unlike organic donors, semiconducting QDs provide a reservoir of electrons that can be more easily donated to an appropriate electron acceptor. Examples of this can be found in the photovoltaics literature, where ET efficiencies remain significant despite the use of saturated ligands to stabilize the QDs.[31,44]

The failure to detect ET, even in the shortest dyads, suggests that our molecular engineering approach to directly probe CISS at the molecular level in organic dyads needs to be deeply reconsidered. Specifically, although most studies on the CISS effect were based on the use of chiral layers containing peptide bridges,[3,4,6b,7,8,16,45] our results show that new molecular approaches are required to simultaneously achieve rapid, efficient ET and efficient CISS-mediated spin filtering in fully organic D-χ-A dyads.

A first approach may rely on *chiral D*-bridge-A dyads, where the CISS filtering potential is provided by D rather than the bridge. This approach could help avoid the constraints imposed by using a saturated chiral bridge, thereby allowing the tuning of the ET efficiency independently from the spin filtering. It would allow adjusting different bridge lengths and types to achieve the perfect match between good ET efficiency and slow charge recombination rate. Promising examples of *chiral D*s are helicenes, which have recently shown good spin filtering properties despite their short length.[46] In a similar approach, one may envision using a *chiral A*. In this case, following the photoexcitation of A, the spin polarisation would arise from the photoinduced hole transfer from A to D.[12b,20a] Another strategy may rely on the use of unsaturated chiral bridges. In this way, the bridge could be engineered to ensure good ET efficiency and slow charge recombination. For instance, aromatic oligoamide foldamers have provided optical evidence of long-distance ET, but no trEPR investigations are reported.[47] Notably, long-lived CT states could also be achieved by the use of D-A-A′ triads.[12b] Even if limited information regarding the CISS filtering efficiency of these chiral molecules is available in the literature, their investigation could help address the fundamental issue of poor ET efficiency observed in the present work with chiral

peptides, which are the gold standard for spintronic detection of CISS.[48]

Conclusions

In summary, we engineered and synthesized six fully organic D-χ-A dyads comprising Py as D and C_{60} as A. Different chiral peptide bridges (χ) were used to investigate the influence of their length and electric dipole orientation on the spin-polarized ET. Through the combination of CV, steady-state and time-resolved optical techniques, we characterized our systems with the ultimate aim of probing a CISS-mediated ET via trEPR spectroscopy. The absence of any detectable ET in both trEPR and TA experiments highlighted a critical gap between our novel spectroscopic approach and state-of-the-art experiments for measuring CISS. In particular, while chiral peptides are extensively used in transport measurements, they are inefficient mediators of intramolecular ET when incorporated into fully organic D-χ-A dyads, even those with a highly favourable energy alignment of the D/A pair.

The observation of CISS effect at the intramolecular level by spectroscopic techniques would significantly advance our understanding of the phenomenon. However, our results show that designing suitable molecular architectures is very demanding, especially when a fully organic approach is followed to gain improved control over photophysical processes. Identifying alternative chiral units that combine efficient ET and good spin filtering ability is a current challenge and a required step to get new insight into the fundamental principles of the CISS effect. In turn, this would help disclose the molecular parameters which underlay effective spin-filtering and promote better engineering of CISS-based molecules needed for the future of CISS-based devices.

Experimental Section

Details on the synthesis and characterization of **Py-Dir**, **Dir4**, **Dir10**, **Dir14**, **Py-Inv**, **Inv4**, **Inv10**, **Py-Inv′**, and **Inv14** are presented in Supporting Information. See Figure 1 and synthetic Schemes S1–S4 for the molecular structures.

Electrochemical measurements

CV was performed in a classic three-electrode cell (working electrode (WE): glassy carbon, diameter 2 mm; counter electrode: platinum wire; reference electrode: Ag wire). The Ag wire was used as a quasi-reference electrode and calibrated at the end of every experiment against the Fc^+/Fc redox couple. Experiments were carried out under Ar atmosphere on degassed 1-mM solutions of the compounds in anhydrous DMSO/toluene (1 : 1 v/v) containing 0.1 M $TBABF_4$ as electrolyte, using an AUTOLAB PGSTAT type III potentiostat/galvanostat and NOVA software from Metrohm Autolab. The WE was mechanically polished before each experiment with 50 nm alumina, followed by electropolishing.

UV-vis absorption and PL

UV-vis absorption spectra were recorded at 25 °C by means of Perkin–Elmer Lambda 45 spectrophotometer. Quartz cuvettes with optical path length of 1 cm were used. The fluorescence spectra were recorded with an Edinburgh FLS920 equipped with a photomultiplier Hamamatsu R928P. The same instrument connected to a PCS900 PC card was used for the trPL experiments, based on the time-correlated single photon counting technique (excitation wavelength $\lambda_{exc} = 330$ nm, emission wavelengths $\lambda_{em} = 395$ and 465 nm). Luminescence quantum yields (±15% uncertainty) were determined using quinine sulfate in diluted sulfuric acid as a reference ($\Phi_{PL} = 0.50$). Emission intensities were corrected for inner filter effects according to standard methods. The optical measurements were performed in pure DMSO (approximate concentration 5 μM).

TrEPR measurements

All trEPR spectra were recorded on a Bruker Elexsys E580 X-band spectrometer equipped with a dielectric ring resonator (ER 4118X-MD5). The sample temperature was maintained using a helium gas-flow cryostat Oxford Instruments CF9350 and controlled with an Oxford Instruments ITC503. Laser excitation was provided by a Litron AURORA II opto-parametric oscillator (OPO) tuneable laser (model number: A23-39-21, 21 Hz repetition rate, *E*/pulse ≈2 mJ, $\lambda = 355$ nm, pulse duration = 7 ns). The laser beam was coupled to the resonator through an optical window. No effects of laser beam polarisation are detected, which suggests the laser beam is non-polarised at sample position. trEPR experiments were performed by direct detection with the transient recorder without lock-in amplification. The instrument response time was about 200 ns. The spectra were acquired with 2 mW microwave power and averaging 100 transient signals at each field position. The magnetic field was measured with a Bruker ER035M NMR gaussmeter.

The trEPR measurements were performed on four dyads, i.e., **Dir14**, **Inv4**, **Inv10**, and **Inv14**. Different solvents were probed (DMSO/toluene, DMF, and toluene) to test how the solvent affects the ET efficiency. Since no significant differences were detected, in the text we report only the measurements in DMSO/toluene (1 : 1 v/v), in line with the TA measurements and electrochemical studies. To avoid aggregation, the concentration of the solutions was 20 μM. The solutions were poured inside EPR quartz tubes that were sealed with Teflon under dinitrogen atmosphere.

After data acquisition, baseline correction in both time and field dimensions was performed. First, we subtracted the pre-trigger offset for each field point; second, we filtered out the laser-induced background signal by subtracting the off-resonance signal intensity from the spectra at each time point. From the data set obtained, the transient EPR spectrum at different time delays after the laser pulse was extracted. The reported trEPR spectra have been averaged over a time window of 0.2 μs.

TA measurements

Femtosecond and nanosecond transient absorption (fsTA and nsTA) spectroscopy was conducted using an apparatus described previously.[49] Briefly, TA spectra and kinetics were acquired using a regeneratively amplified Ti:sapphire laser system (Tsunami oscillator/Spitfire amplifier (Spectra-Physics)) to pump a commercial collinear optical parametric amplifier (TOPAS-Prime, Light-Conversion LLC) to generate 350 nm laser pulses.[49] Before interaction with the sample, the probe was split using a neutral density filter so that one portion interacted with the sample and one portion provided a reference spectrum. The pump (350 nm, 1 μJ/pulse, 120 fs) was sent

through a commercial depolarizer (DPU-25-A, Thorlabs, Inc.) to suppress the effects of rotational dynamics and chopped at 500 Hz. The pump was focused to about 0.2 mm diameter and the probe to about 0.1 mm diameter at the sample. The reference probe and the transmitted probe were coupled into optical fibers and detected using a customized Helios spectrometer and Helios software (Ultrafast Systems, LLC). NsTA spectroscopy experiments were performed using the pump pulse described for the fsTA experiments paired with a photonic crystal fiber ultra-broadband probe generated by a customized EOS spectrometer (Ultrafast Systems, LLC). The temporal resolution was about 120–280 fs in the fsTA experiments and about 600–900 ps in the nsTA experiments. FsTA and nsTA spectra were collected for 3 s at each pump-probe time delay.

Samples of the dyads and control compounds were dissolved in DMSO/toluene (1:1 v/v) and prepared with an optical density of 0.8 at 350 nm in 2 mm quartz cuvettes fused to a glass bulb. This bulb was used to subject each sample to three freeze-pump-thaw cycles under vacuum (10^{-4} Torr) to remove oxygen. Samples were stirred to minimize the effects of local heating and degradation. Visible and near-infrared data were individually chirp-corrected (Surface Xplorer 4, Ultrafast Systems, LLC), and fsTA and nsTA data were merged in MATLAB prior to kinetic analysis. Data were analyzed using lab-written, selected-wavelength global fitting software.[50] The errors of the lifetimes given in the figures are derived from the standard deviations from the global fitting propagated with the uncertainty described by the instrument response (0.3 ps and 0.8 ns for fsTA and nsTA, respectively).

Author Contributions

A.P.: investigation (EPR spectroscopy), formal analysis, project administration, writing original draft, writing review and editing.

D. F.: synthesis, formal analysis, writing original draft.

De. G.: synthesis, formal analysis, writing original draft and editing.

E. I. L.: investigation (transient absorption), formal analysis, writing original draft and editing.

Da. G.: investigation (UV-vis absorption and PL), formal analysis, writing original draft and editing.

F. T.: investigation (electrochemistry), formal analysis, writing original draft and editing.

L. M.: investigation (UV-vis absorption and PL), formal analysis.

M. C.: conceptualization, supervision (EPR), writing review and editing.

C. F.: supervision (electrochemistry), writing review and editing.

E. S.: supervision (EPR), writing review and editing.

A. C.: conceptualization, supervision (electrochemistry), writing original draft, writing review and editing.

M. W.: supervision (transient absorption), fund acquisition, writing original draft, writing review and editing.

C. T.: conceptualization, supervision (synthesis), project administration, writing original draft, writing review and editing.

R.S.: conceptualization, supervision, project administration, fund acquisition, writing original draft, writing review and editing.

Acknowledgements

This work has received funding from the Italian Ministry of University and Research (MUR) through PRIN Project 2017CR5WCH Q-ChiSS ''Quantum detection of chiral-induced spin selectivity at the molecular level'' and "Progetto Dipartimenti di Eccellenza 2018–2022 (ref. no. B96C1700020008) and by the US National Science Foundation under award #CHE-2154627 (M.R.W., transient absorption measurements). A.P. acknowledges funding by MUR under the National Recovery and Resilience Plan (NRRP), Mission 4 Component 2 Investment 1.2–Call for tender No. 247 of 19/08/2022 (Project ID: SOE_0000064, Photodriven spin selectivity in chiral organic molecules and devices–PHOTOCODE). A. C. and F. T. are grateful to Prof. Marco Borsari (University of Modena and Reggio Emilia) for stimulating discussion on electrochemical measurements. Co-funded by the European Union (ERC SyG, CASTLE, 101071533). Views and opinions expressed are however those of the author(s) only and do not necessarily reflect those of the European Union or the European Research Council. Neither the European Union nor the granting authority can be held responsible for them.

Conflict of Interests

The authors declare no conflicts of interest.

Data Availability Statement

The data that support the findings of this study are available from the corresponding author upon reasonable request.

Keywords: CISS effect · donor/acceptor dyads · electron transfer · photophysics · polypeptide

[1] A. Guijarro, *The Origin of Chirality in the Molecules of Life: From Awareness to the Current Theories and Perspectives of this Unsolved Problem*, Royal Society of Chemistry, **2022**.
[2] K. Ray, S. P. Ananthavel, D. H. Waldeck, R. Naaman, *Science* **1999**, *283*, 814–816.
[3] R. Naaman, Y. Paltiel, D. H. Waldeck, *Nat. Chem. Rev.* **2019**, *3*, 250–260.
[4] a) R. Naaman, Y. Paltiel, D. H. Waldeck, *J. Phys. Chem. Lett.* **2020**, *11*, 3660–3666; b) D. H. Waldeck, R. Naaman, Y. Paltiel, *APL Materials* **2021**, *9*, 040902; c) F. Evers, A. Aharony, N. Bar-Gill, O. Entin-Wohlman, P. Hedegård, O. Hod, P. Jelinek, G. Kamieniarz, M. Lemeshko, K. Michaeli, V. Mujica, R. Naaman, Y. Paltiel, S. Refaely-Abramson, O. Tal, J. Thijssen, M. Thoss, J. M. van Ruitenbeek, L. Venkataraman, D. H. Waldeck, B. Yan, L. Kronik, *Adv. Mater.* **2022**, *34*, 2106629.
[5] Y.-H. Kim, Y. Zhai, H. Lu, X. Pan, C. Xiao, E. A. Gaulding, S. P. Harvey, J. J. Berry, Z. V. Vardeny, J. M. Luther, M. C. Beard, *Science* **2021**, *371*, 1129–1133.
[6] a) A. Chiesa, M. Chizzini, E. Garlatti, E. Salvadori, F. Tacchino, P. Santini, I. Tavernelli, R. Bittl, M. Chiesa, R. Sessoli, S. Carretta, *J. Phys. Chem. Lett.*

2021, *12*, 6341–6347; b) S.-H. Yang, R. Naaman, Y. Paltiel, S. S. P. Parkin, *Nat. Rev. Phys.* **2021**, *3*, 328–343; c) A. Privitera, M. Righetto, F. Cacialli, M. K. Riede, *Adv. Opt. Mater.* **2021**, *9*, 2100215.
[7] C. D. Aiello, J. M. Abendroth, M. Abbas, A. Afanasev, S. Agarwal, A. S. Banerjee, D. N. Beratan, J. N. Belling, B. Berche, A. Botana, J. R. Caram, G. L. Celardo, G. Cuniberti, A. Garcia-Etxarri, A. Dianat, I. Diez-Perez, Y. Guo, R. Gutierrez, C. Herrmann, J. Hihath, S. Kale, P. Kurian, Y.-C. Lai, T. Liu, A. Lopez, E. Medina, V. Mujica, R. Naaman, M. Noormandipour, J. L. Palma, Y. Paltiel, W. Petuskey, J. C. Ribeiro-Silva, J. J. Saenz, E. J. G. Santos, M. Solyanik-Gorgone, V. J. Sorger, D. M. Stemer, J. M. Ugalde, A. Valdes-Curiel, S. Varela, D. H. Waldeck, M. R. Wasielewski, P. S. Weiss, H. Zacharias, Q. H. Wang, *ACS Nano* **2022**, *16*, 4989–5035.
[8] J. M. Abendroth, D. M. Stemer, B. P. Bloom, P. Roy, R. Naaman, D. H. Waldeck, P. S. Weiss, P. C. Mondal, *ACS Nano* **2019**, *13*, 4928–4946.
[9] T. S. Metzger, S. Mishra, B. P. Bloom, N. Goren, A. Neubauer, G. Shmul, J. Wei, S. Yochelis, F. Tassinari, C. Fontanesi, D. H. Waldeck, Y. Paltiel, R. Naaman, *Angew. Chem. Int. Ed.* **2020**, *59*, 1653–1658.
[10] P. C. Mondal, C. Fontanesi, D. H. Waldeck, R. Naaman, *Acc. Chem. Res.* **2016**, *49*, 2560–2568.
[11] W. Mtangi, F. Tassinari, K. Vankayala, A. Vargas Jentzsch, B. Adelizzi, A. R. A. Palmans, C. Fontanesi, E. W. Meijer, R. Naaman, *J. Am. Chem. Soc.* **2017**, *139*, 2794–2798.
[12] a) A. Privitera, E. Macaluso, A. Chiesa, A. Gabbani, D. Faccio, D. Giuri, M. Briganti, N. Giaconi, F. Santanni, N. Jarmouni, L. Poggini, M. Mannini, M. Chiesa, C. Tomasini, F. Pineider, E. Salvadori, S. Carretta, R. Sessoli, *Chem. Sci.* **2022**, *13*, 12208–12218; b) S. M. Harvey, M. R. Wasielewski, *JACS* **2021**, *143*, 15508–15529; c) A. Chiesa, A. Privitera, E. Macaluso, M. Mannini, R. Bittl, R. Naaman, M. R. Wasielewski, R. Sessoli, S. Carretta, *Adv. Mater.* 2300472.
[13] a) T. P. Fay, D. T. Limmer, *Nano Lett.* **2021**, *21*, 6696–6702; b) T. P. Fay, D. T. Limmer, *J. Chem. Phys.* **2023**, *158*.
[14] T. P. Fay, *J. Phys. Chem. Lett.* **2021**, *12*, 1407–1412.
[15] J. Luo, P. J. Hore, *New J. Phys.* **2021**, *23*, 043032.
[16] R. Naaman, Y. Paltiel, D. H. Waldeck, *Acc. Chem. Res.* **2020**, *53*, 2659–2667.
[17] T. M. Figueira-Duarte, K. Müllen, *Chem. Rev.* **2011**, *111*, 7260–7314.
[18] a) G. Zaragoza-Galán, J. Ortíz-Palacios, B. X. Valderrama, A. A. Camacho-Dávila, D. Chávez-Flores, V. H. Ramos-Sánchez, E. Rivera, *Molecules* **2014**, *19*, 352–366; b) M. I. Sluch, I. D. W. Samuel, M. C. Petty, *Chem. Phys. Lett.* **1997**, *280*, 315–320; c) S. Fujii, T. Morita, S. Kimura, *Langmuir* **2008**, *24*, 5608–5614; d) A. S. D. Sandanayaka, Y. Araki, O. Ito, G. R. Deviprasad, P. M. Smith, L. M. Rogers, M. E. Zandler, F. D'Souza, *Chem. Phys.* **2006**, *325*, 452–460.
[19] M. Prato, *in Fullerenes and Related Structures* (Ed.: A. Hirsch), Springer Berlin Heidelberg, Berlin, Heidelberg, **1999**, pp. 173–187.
[20] a) I. Ramirez, A. Privitera, S. Karuthedath, A. Jungbluth, J. Benduhn, A. Sperlich, D. Spoltore, K. Vandewal, F. Laquai, M. Riede, *Nat. Commun.* **2021**, *12*, 471; b) B. C. Thompson, J. M. J. Fréchet, *Angew. Chem. Int. Ed.* **2008**, *47*, 58–77; c) J. Niklas, S. Beaupré, M. Leclerc, T. Xu, L. Yu, A. Sperlich, V. Dyakonov, O. G. Poluektov, *J. Phys. Chem. B* **2015**, *119*, 7407–7416; d) A. Privitera, M. Righetto, D. Mosconi, F. Lorandi, A. A. Isse, A. Moretto, R. Bozio, C. Ferrante, L. Franco, *Phys. Chem. Chem. Phys.* **2016**, *18*, 31286–31295; e) A. Privitera, J. Grüne, A. Karki, W. K. Myers, V. Dyakonov, T.-Q. Nguyen, M. K. Riede, R. H. Friend, A. Sperlich, A. J. Gillett, *Adv. Energy Mater.* **2022**, *12*, 2103944.
[21] B. P. Bloom, B. M. Graff, S. Ghosh, D. N. Beratan, D. H. Waldeck, *JACS* **2017**, *139*, 9038–9043.
[22] C. Tomasini, G. Luppi, M. Monari, *JACS* **2006**, *128*, 2410–2420.
[23] C. Clever, E. Wierzbinski, B. P. Bloom, Y. Lu, H. M. Grimm, S. R. Rao, W. S. Horne, D. H. Waldeck, *Isr. J. Chem.* **2022**, *62*, e202200045.
[24] a) L. Garbuio, S. Antonello, I. Guryanov, Y. Li, M. Ruzzi, N. J. Turro, F. Maran, *JACS* **2012**, *134*, 10628–10637; b) E. Galoppini, M. A. Fox, *JACS* **1996**, *118*, 2299–2300.
[25] K. Kordatos, T. Da Ros, S. Bosi, E. Vázquez, M. Bergamin, C. Cusan, F. Pellarini, V. Tomberli, B. Baiti, D. Pantarotto, V. Georgakilas, G. Spalluto, M. Prato, *J. Org. Chem.* **2001**, *66*, 4915–4920.
[26] E. M. Espinoza, J. A. Clark, J. B. Derr, D. Bao, B. Georgieva, F. H. Quina, V. I. Vullev, *ACS Omega* **2018**, *3*, 12857–12867.
[27] J. F. O'Donnell, C. K. Mann, *J. Electroanal. Chem. Interfacial Electrochem.* **1967**, *13*, 157–162.
[28] a) A. Menon, J. A. H. Dreyer, J. W. Martin, J. Akroyd, J. Robertson, M. Kraft, *Phys. Chem. Chem. Phys.* **2019**, *21*, 16240–16251; b) B. P. Klein, L. Ruppenthal, S. J. Hall, L. E. Sattler, S. M. Weber, J. Herritsch, A. Jaegermann, R. J. Maurer, G. Hilt, J. M. Gottfried, *ChemPhysChem* **2021**, *22*, 1065–1073; c) D. Vanossi, L. Cigarini, A. Giaccherini, E. Da Como, C. Fontanesi, *Molecules* **2016**, *21*, 110.
[29] M. M. Islam, Z. Hu, Q. Wang, C. Redshaw, X. Feng, *Mater. Chem. Front.* **2019**, *3*, 762–781.
[30] a) D. Genovese, E. Rampazzo, S. Bonacchi, M. Montalti, N. Zaccheroni, L. Prodi, *Nanoscale* **2014**, *6*, 3022–3036; b) A. O. Ba-Salem, J. Duhamel, *Langmuir* **2021**, *37*, 6069–6079.
[31] M. Righetto, A. Privitera, F. Carraro, L. Bolzonello, C. Ferrante, L. Franco, R. Bozio, *Nanoscale* **2018**, *10*, 11913–11922.
[32] J. Daub, R. Engl, J. Kurzawa, S. E. Miller, S. Schneider, A. Stockmann, M. R. Wasielewski, *J. Phys. Chem. A* **2001**, *105*, 5655–5665.
[33] H. Mao, R. M. Young, M. D. Krzyaniak, M. R. Wasielewski, *J. Phys. Chem. B* **2022**, *126*, 10519–10527.
[34] R. M. Hochstrasser, S. K. Lower, *J. Chem. Phys.* **1964**, *40*, 1041–1046.
[35] A. Sassara, G. Zerza, M. Chergui, *Chem. Phys. Lett.* **1996**, *261*, 213–220.
[36] a) V. I. Vullev, G. Jones, *Res. Chem. Intermed.* **2002**, *28*, 795–815; b) G. Jones Ii, X. Zhou, V. I. Vullev, *PPS* **2003**, *2*, 1080–1087.
[37] a) C. Zuliani, F. Formaggio, L. Scipionato, C. Toniolo, S. Antonello, F. Maran, *ChemElectroChem.* **2020**, *7*, 1225–1237; b) M. Sisido, S. Hoshino, H. Kusano, M. Kuragaki, M. Makino, H. Sasaki, T. A. Smith, K. P. Ghiggino, *J. Phys. Chem. B* **2001**, *105*, 10407–10415; c) R. A. Marcus, N. Sutin, *Biochim. Biophys. Acta* **1985**, *811*, 265–322.
[38] a) S. S. Isied, M. Y. Ogawa, J. F. Wishart, *Chem. Rev.* **1992**, *92*, 381–394; b) I. Ron, I. Pecht, M. Sheves, D. Cahen, *Acc. Chem. Res.* **2010**, *43*, 945–953.
[39] a) R. Bittl, S. Weber, *Biochim. Biophys. Acta Bioenerg.* **2005**, *1707*, 117–126; b) W. Lubitz, F. Lendzian, R. Bittl, *Acc. Chem. Res.* **2002**, *35*, 313–320; c) H. Levanon, K. Möbius, *Annu. Rev. Biophys. Biomol. Struct.* **1997**, *26*, 495–540.
[40] a) D. Gust, T. A. Moore, A. L. Moore, *Acc. Chem. Res.* **1993**, *26*, 198–205; b) M. R. Wasielewski, *Chem. Rev.* **1992**, *92*, 435–461.
[41] Z. E. X. Dance, Q. Mi, D. W. McCamant, M. J. Ahrens, M. A. Ratner, M. R. Wasielewski, *J. Phys. Chem. B* **2006**, *110*, 25163–25173.
[42] H. Overing, M. N. Paddon-Row, M. Heppener, A. M. Oliver, E. Cotsaris, J. W. Verhoeven, N. S. Hush, *J. Am. Chem. Soc.* **1987**, *109*, 3258–3269.
[43] B. Albinsson, J. Mårtensson, *Journal of Photochemistry and Photobiology C: Photochemistry Reviews* **2008**, *9*, 138–155.
[44] a) G. H. Carey, A. L. Abdelhady, Z. Ning, S. M. Thon, O. M. Bakr, E. H. Sargent, *Chem. Rev.* **2015**, *115*, 12732–12763; b) A. Privitera, M. Righetto, R. Bozio, L. Franco, *MRS Advances* **2017**, 1–9; c) R. Wang, Y. Shang, P. Kanjanaboos, W. Zhou, Z. Ning, E. H. Sargent, *Energy Environ. Sci.* **2016**, *9*, 1130–1143.
[45] K. Michaeli, N. Kantor-Uriel, R. Naaman, D. H. Waldeck, *Chem. Soc. Rev.* **2016**, *45*, 6478–6487.
[46] a) Y. Liang, K. Banjac, K. Martin, N. Zigon, S. Lee, N. Vanthuyne, F. A. Garcés-Pineda, J. R. Galán-Mascarós, X. Hu, N. Avarvari, M. Lingenfelder, *Nat. Commun.* **2022**, *13*, 3356; b) M. Kettner, V. V. Maslyuk, D. Nürenberg, J. Seibel, R. Gutierrez, G. Cuniberti, K.-H. Ernst, H. Zacharias, *J. Phys. Chem. Lett.* **2018**, *9*, 2025–2030; c) V. Kiran, S. P. Mathew, S. R. Cohen, I. Hernández Delgado, J. Lacour, R. Naaman, *Adv. Mater.* **2016**, *28*, 1957–1962.
[47] X. Li, N. Markandeya, G. Jonusauskas, N. D. McClenaghan, V. Maurizot, S. A. Denisov, I. Huc, *JACS* **2016**, *138*, 13568–13578.
[48] S. Mishra, A. K. Mondal, S. Pal, T. K. Das, E. Z. B. Smolinsky, G. Siligardi, R. Naaman, *J. Phys. Chem. C.* **2020**, *124*, 10776–10782.
[49] R. M. Young, S. M. Dyar, J. C. Barnes, M. Juricek, J. F. Stoddart, D. T. Co, M. R. Wasielewski, *J. Phys. Chem. A* **2013**, *117*, 12438–12448.
[50] I. Roy, S. Bobbala, Y. Beldjoudi, M. T. Nguyen, R. M. Young, M. M. Cetin, J. A. Cooper, S. Allen, O. Anamimoghadam, E. A. Scott, M. R. Wasielewski, J. F. Stoddart, *J. Am. Chem. Soc.* **2019**, *141* 12296–12304.

Manuscript received: March 29, 2023
Accepted manuscript online: September 7, 2023
Version of record online: October 20, 2023